Automatic detection of wildfire burn scars and estimation of greenhouse gas emissions in the Chapada dos Guimarães environmental protection area using satellite images

Robson Brito Santos[1], Igor Luiz Berti Silva[2], Thiago Statella[3]

[1] Instituto Federal de Educação, Ciência e Tecnologia de São Paulo, Campus Presidente Epitácio. Graduando em Ciências da Computação. https://orcid.org/0009-0002-2154-3891. E-mail: robsonbrito.santos@outlook.com

[2] Instituto Federal de Educação, Ciência e Tecnologia de São Paulo, Campus Presidente Epitácio. Graduado em Ciências da Computação. https://orcid.org/0009-0007-2084-0858. E-mail: igorluizb.silva@gmail.com

[3] Instituto Federal de Educação, Ciência e Tecnologia de São Paulo, Campus Presidente Epitácio. Doutor em Ciências Cartográficas. https://orcid.org/0000-0002-8656-9147. E-mail: t.statella@gmail.com

Received in: 26/02/2025
Accepted in: 28/06/2025

Abstract

Wildfires are recurrent in the Chapada dos Guimarães environmental protection area, Mato Grosso, Brazil. Besides the fact that these fires significantly affect biogeochemical cycles, another cause for concern is the release of greenhouse gases such as CO_2, CH_4 and N_2O from biomass burning. Thus, this study was developed to create a computer system for detecting wildfire burn scars and measuring the volume of gases released automatically. Construction was based on the calculation of spectral indices from Sentinel-2 images, with a spatial resolution of 10 meters and a five-day time resolution. The system downloads data every five days, generates a thematic map showing burned areas and a report in CSV format with area size and an estimate of emitted gases. It is currently operational and constantly monitors the appearance of new points of origin in the study area. Validation to date is qualitative, but a quantitative approach is underway.

Keywords: Remote sensing. Fire detection. Greenhouse gases.

Introduction

The environmental protection area (PA) of the Chapada dos Guimarães National Park was created in 1995 by Decree No. 537, of November 21, 1995. Oversaw by the state of Mato Grosso, the PA extends over 251,848 hectares that cover the municipalities of Cuiabá (35.7%), Campo Verde (1.6%), Santo Antônio do Leverger (11%) and Chapada dos Guimarães (51.7%). Within the borders of the *Cerrado* biome, the protection area houses several endangered species (Machado *et al.*, 2004), showing a great diversity of reliefs and is part of the Upper Paraguay River basin, in addition to sheltering springs of the Cuiabá River, one of the main sources of the Mato Grosso Pantanal. Among the vegetative physiognomies found in the park are riparian forest, gallery forest, dry forest, *Cerradão*, *Cerrado strictu sensu* (dense *Cerrado*, typical *Cerrado*, rupestrian *Cerrado*), dirty field, clean field, *vereda* and palm grove (Sano *et al.*, 2008).

Although the typical *Cerrado* formations are well adapted to wildfires, the Management Plan for Chapada dos Guimarães National Park, conducted by the Chico Mendes Institute for Biodiversity Conservation (ICMBio, 2009), cites wildfire as one of the main threats to the region's vegetation, especially those of criminal origin. Especially during the dry season, unnatural wildfires can drastically and permanently alter the structure and floristic composition of vegetation (Arruda *et al.*, 2016; Fiedler *et al.*, 2006; Shimabukuro *et al.*, 2020). Moreover, fires such as the one that occurred in 2019, which destroyed an area of approximately 4,000 hectares (according to ICMBio), can cause indirect damage like erosion, loss of soil fertility, and major disruption to local wildlife.

According to ICMBio (2009), large wildland fires involving areas of up to 30,000 hectares (such as the one that occurred in 1994, which affected about 90% of Chapada dos Guimarães National Park) occur with alarming frequency every year. Regarding the period of occurrence, most fires (around 98%) are recorded between July and October, with the highest incidence in September (45% of the total) and August (41% of the total). Given that most points of origin recorded in the park occur during the dry season and are caused by human activity, it is clear that this factor poses a threat to vegetation and fauna, altering natural ecological processes.

Besides the fires significantly affecting biogeochemical cycles, surface energy balance, atmospheric radiation balance, and the hydrological cycle (Pereira et al., 2012), another cause for concern is the release of greenhouse gases such as carbon dioxide (CO_2), methane (CH_4), and nitrous oxide (N_2O) from biomass burning. It is globally agreed (see the Paris Agreement, 2015) that countries need to adopt carbon emission reduction strategies, otherwise they risk causing or exacerbating climate change due to the imbalance between atmospheric constituents (Galanter *et al.*, 2000; Kaufman *et al.*, 1992; Langmann *et al.*, 2009; Urbanski, 2014). Its main promoter is the Intergovernmental Panel on Climate Change (IPCC). Among the IPCC activities are the creation, formatting and publication of the IPCC Guidelines for National Greenhouse Gas Inventories, which proposes methodologies for quantifying and compiling a global inventory of gas emissions.

Estimates of greenhouse gas emissions can be made by indirect measurements, using remote sensors data (Chen *et al.*, 2024). According to them, remote data plays an essential role in wildfire monitoring, ranging from pre-fire conditions to post-fire impacts. The authors discuss recent technologies for determining burned areas and emissions, and address challenges such as the need for consistent and continuous long-term data while exploring future opportunities in fire management. In this regard, they emphasize the importance of using sensing data and the IPCC methodology for estimating greenhouse gases.

It is clear, therefore, that using remote sensors to identify wildfires and quantify emissions is a robust methodology which can be applied to monitor wildfires in the Chapada dos Guimarães PA and to inventory greenhouse gas emissions into the atmosphere, in accordance with the IPCC guidelines. By using geotechnologies like Geographic Information Systems (Chuvieco *et al.*, 2019) and data from remote sensors and cartographic documents, a timeline can be established during which greenhouse gas emissions will be estimated and used to build an annual inventory of CO_2, CH_4, and N_2O emissions.

Given this context, this study was developed to create an automated system to identify and quantify, based on orbital images, areas with wildfire burn scars in the Chapada dos Guimarães PA, and to estimate greenhouse gas emissions in a systematic manner, following IPCC specifications.

Material and methods

In short, the method adopted consists of constructing an image bank with frames from the study region, detecting burned areas, calculating gas emissions over time and analyzing the results, according to the flowchart presented in Figure 1.

Accessing, downloading, importing and processing orbital images for identifying wildfire burn scars and quantifying greenhouse gas emissions were automated using routines written in Python language, integrated with the Geographic Information System (GIS) GRASS (Geographical Resources Analysis Support System), a free software available under the GNU General Public License (GPL).

Figure 1. Execution flowchart.

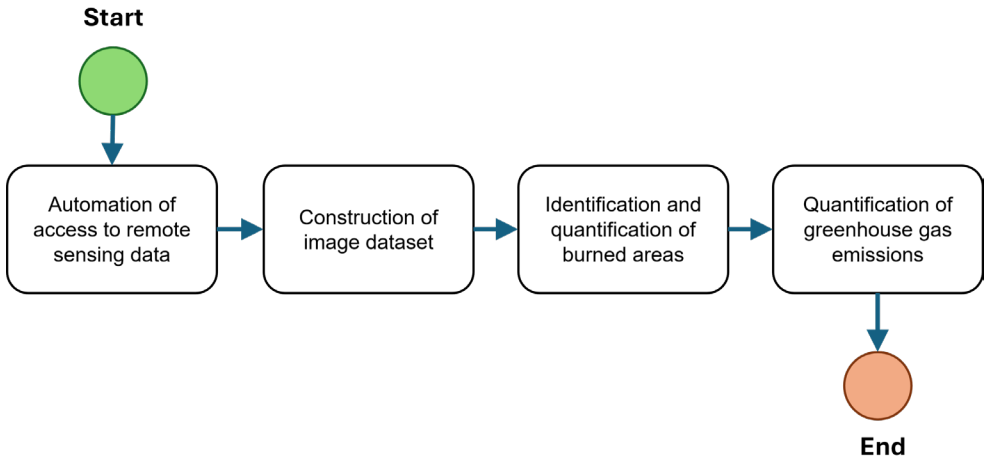

Source: authors (2024).

The orbital platform adopted was Sentinel-2, from the European Space Agency (ESA), obtained free of charge via a service offered by the Copernicus Data Space Ecosystem (CDSE). Two Sentinel-2 satellites, identified by the suffixes A and B, were launched in 2015 and 2021, respectively. Both have MultiSpectral Instrument (MSI) sensors that capture data in 13 spectral bands, with spatial resolution of up to 10 meters and a five-day time resolution. The high temporal resolution enables more effective monitoring of fire occurrences in the study area. The Sentinel-2 images used have L2A processing level, the highest available, in which data undergo geometric and radiometric correction, are converted to reflectance, and corrected for atmospheric scattering and absorption effects and effects caused by terrain.

Each pixel attribute in these images can therefore be considered surface reflectance, which enables adequate spectral analysis. B4 (red), B8 (near infrared) and B12 (shortwave infrared) were the bands used. For complete coverage of the study area, two frames are required in each orbit (two quadrangles), which are mosaicked and resampled. This is done so that band 12, with a 20-meter resolution, can be used in map calculations with other bands, which have a resolution of 10 meters. Spectral ranges of each band and their spatial resolution, as provided by the CDSE (Figure 2), are illustrated, showing the platform's enhanced detection and monitoring capabilities, which are essential for detailed environmental assessments.

Identifying candidate pixels for the wildfire burn scar information class employs the Normalized Burn Ratio (NBR), used to highlight vegetated areas that were burnt (Chuvieco *et al.*, 2019; Pleniou and Koutsias, 2013), based on equation 1.

$$NBR = \frac{\rho_{B8} - \rho_{B12}}{\rho_{B8} + \rho_{B12}} \quad (1)$$

In which: ρ_{B8} and ρ_{B12} are surface reflectance in the near infrared and shortwave bands, respectively.

Reflectance in the near infrared band is expected to be drastically reduced while reflectance in the shortwave infrared will increase for fire scar pixels. Hence, equation 1 produces negative values for pixels that are candidates for the fire scar class (Pleniou and Koutsias, 2013). Nonetheless, false positives can occur in areas of well-drained exposed soil, which often have negative NBR values. To reduce the occurrence of false positives, only pixels with values $NBR \leftarrow 0{,}2$ were considered as belonging to burned areas. The set of pixels that meets this restriction is used to calculate the total burned area.

Figure 2. Sentinel-2 bands and their spatial resolutions.

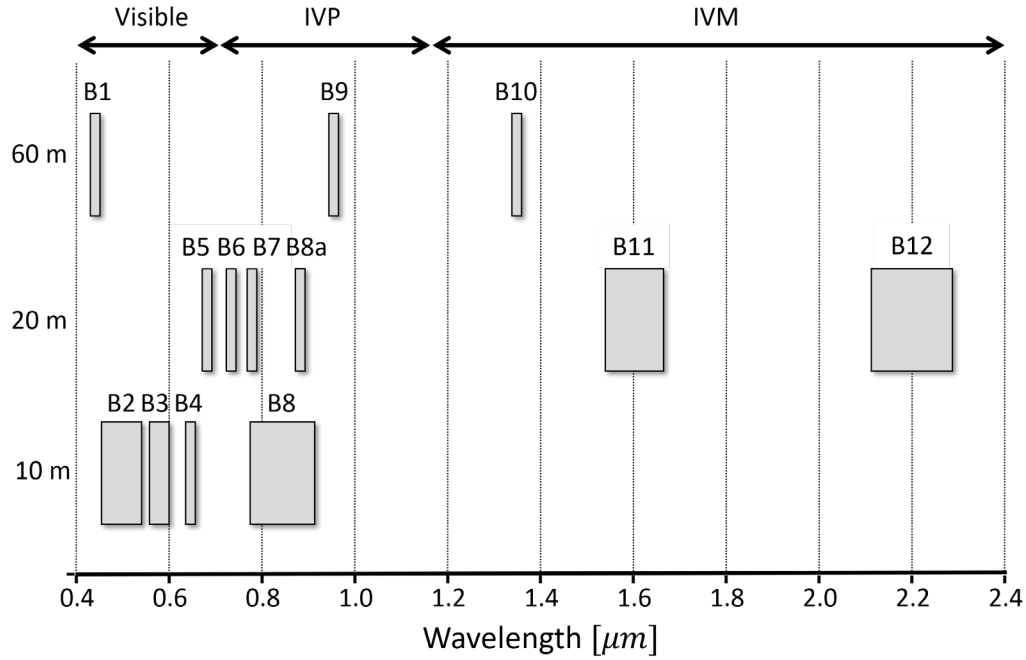

Source: authors (2024).

Emissions were calculated following the IPCC Guideline 2019, which models the amount (mass) of greenhouse gases FG generated by any type of fire (surface, canopy or complete) in tons, according to equation 2:

$$FG = A \cdot M_B \cdot C_F \cdot G_{ef} \cdot 0{,}001 \quad (2)$$

In which: A is the burned area in hectares (ha), M_B is the available mass of combustion in tons/hectare, C_F is the combustion factor (dimensionless and dependent on the type of vegetation) and G_{ef} is the emission factor of burned dry matter.

Combustion factor measures the proportion of combustible material that is actually burned, which varies depending on the size and architecture of the combustible mass, moisture content of the material, and type of fire. Emission factor gives the volume of emissions of a specific gas per unit of dry matter burned, which can vary depending on the carbon content of the biomass and the completeness of combustion.

IPCC establishes the following sequence for calculation:

1. Characterization of forest areas according to climatic or ecological zones;
2. Estimated available combustion mass M_B in tons/hectare, which includes biomass, wood, and other types of dead organic matter;
3. Select combustion factor C_F and emission factor G_{ef};
4. Apply the parameters to the equation FG for each type of gas.

In equation 2, for simplicity, the IPCC recommends neglecting the contribution of wood and dead organic matter to M_B. Emission G_{ef} and combustion C_F factors can use reference values provided by the IPCC, as shown in Tables 1 and 2.

Fuel amount for burning is determined by the area of the fire and the density of the material present at the site. This density can include biomass and dead organic matter, which vary depending on vegetation type, age and condition. Type of fire also influences the amount of material burned. For example, the fuel available for

Table 1. Reference values for emission factor G_{ef} in g´kg^{-1} for different types of vegetation (IPCC guidelines).

Category	CO_2	CH_4	N_2O
Savanna and Grassland	1.613 ± 95	2.3 ± 0.9	0.21 ± 0.1

Source: adapted from IPCC (2019).

low-intensity ground fires is restricted to organic matter deposited on the ground like leaves and dead wood. In turn, intense fires can consume much of the biomass in the tree canopy. The burned area can be obtained by analyzing remote sensing data. More simply, fuel biomass can be obtained by using standardized values informed by the IPCC. In this case, the value is entered into equation 2 instead of the product $M_B \cdot C_F$. For *Cerrado* type vegetation, the value used is 4.6 t×ha^{-1} with a ± 1.5 t×ha^{-1} accuracy.

Results and discussion

Chapada dos Guimarães PA location is shown in Figure 1. Its area covers two geomorphological units: the Guimarães Plateau and the Paraguay River Depression. The PA vector boundaries in Figure 3, provided by the Mato Grosso Land Institute (INTERMAT), are available in the SIRGAS2000 geodetic reference system and the Mercator cartographic projection system (coordinates in meters). These vector data are fundamental for the management, monitoring, and sustainable planning of the protected area.

Monitoring and quantification of gases released in forest fires can be achieved using remote sensors on aerial or orbital platforms and indirect measurement methods (automatic or visual) that inevitably involve identifying burned areas in digital images. In the use of remote sensor data to identify forest fire scars and active fires, the use of Sentinel, MODIS, and Landsat systems stands out (Alvarado *et al.*, 2017; Bastarrika *et al.*, 2011; Boschetti *et al.*, 2015; Arruda *et al.*, 2021; Argibay *et al.*, 2020; Díaz-Vázquez *et al.*, 2025; Hislop *et al.*, 2020; Laris, 2005; Makineci, 2024; Molema *et al.*, 2025; Olson *et al.*, 1999; Vasconcelos *et al.*, 2013; Wooster *et al.*, 2005; Zhang *et al.*, 2003).

Figure 4 shows a Sentinel-2 image acquired on July 15, 2023 over the study area, in the color composition B4(B)B8(G)B12(R). In this composition, the Red band is represented by the color Blue; the Near Infrared band is represented by the color Green; and the Shortwave Infrared band (or Medium, according to some bibliographies) is represented by the color Red. Images are provided with coordinates

Table 2. Reference values for combustion factor C_f (IPCC guidelines).

Type of vegetation	Subcategory	C_f
Savanna (fires at the beginning of the dry season)	Savanna Forest	0.22
	Savanna Park	0.73
	Other types of Savanna Forest	0.37 ± 0.19
All types of Savanna Forests (fires at the beginning of the dry season)		0.40 ± 0.22
Savanna (fires in the middle/end of the dry season)	Savanna Forest	0.72
	Savanna Park	0.82 ± 0.07
	Tropical Savanna	0.73 ± 0.04
	Other types of Savanna Forest	0.68 ± 0.19
All types of Savanna Forests (fires in the middle/end of the dry season)		0.74 ± 0.14

Source: adapted from IPCC (2019).

Figure 3. Location of the study area.

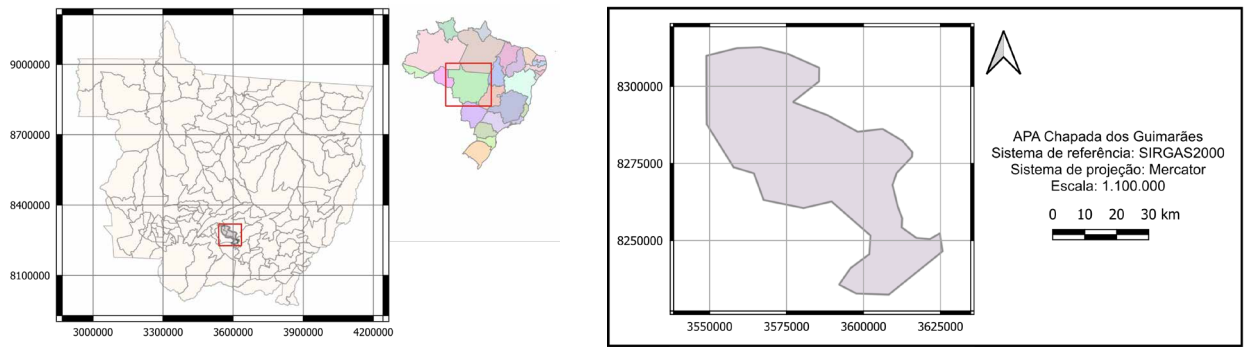

Source: authors (2024).

in the WGS84 geodetic reference system and Universal Transverse Mercator (UTM) projection, zone 21 South.

UTM projection preserves conformity, i.e., it represents angles without scale distortion and therefore preserves the shape of small areas. Given this conformity, the UTM projection is not suitable for this task, since areas and distances cannot be represented without distortion (except, of course, on the secant lines). Thus, after importing the satellite images, they are reprojected on the Equivalent Cylindrical projection, whose main feature is the maintenance of areas in true scale, facilitating the accurate analysis of burned areas and the comparison of different dates.

In the color composition shown in Figure 4 (a mask was applied to isolate only the pixels within the PA boundaries), healthy vegetation appears in shades of green due to high reflectance in the near-infrared band (B8), which results from

Figure 4. Sentinel-2 image in color composition B4(B)B8(G)B12(R).

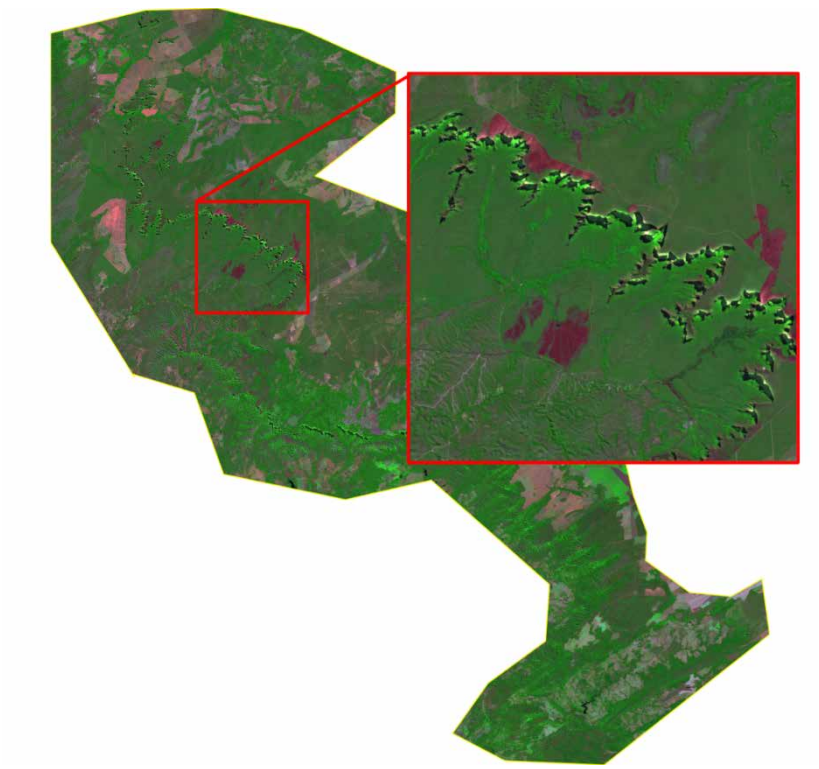

Source: authors (2024).

the interaction of electromagnetic radiation with the spongy mesophyll cells of plants, providing a clear and detailed view of healthy vegetation cover and forest fire-induced changes.

Moreover, comparing images acquired on different dates allows the identification of changes in land cover and the analysis of fire dynamics over time. This enables the assessment of trends in the frequency and intensity of fires, helping to formulate more effective PA management and conservation strategies.

Radiation in the red band (B4) is largely absorbed by chlorophylls and carotenoids for photosynthesis, and reflectance is lower in the shortwave infrared (B12), a band sensitive to vegetation moisture content. Burned areas appear in dark shades of magenta due to increased reflectance in the shortwave infrared and reduced reflectance in the near infrared. Figure 4 pinpoints areas burned by fires that occurred between July 10 and 14, 2023. In addition to their reddish hue, forest fire scars are irregular in shape, except at points where the fire encounters an anthropogenic barrier such as roads. A few points detailed in Figure 4 show that the fire managed to cross some roads. Dry, well-drained soils tend to be represented in magenta as well, but in lighter shades, and can sometimes be confused with forest fire scar areas. Mixed areas, where vegetation is low-lying or does not completely cover the ground, appear in shades of greenish yellow in this colorful composition.

Figure 5 shows reflectance curves for healthy vegetation and for areas where vegetation has been burned (Alcaras *et al.*, 2002). In the visible region, the spectral behavior of vegetation is controlled by plant pigments like chlorophyll and carotenoids. In the near infrared, reflectance is controlled by the plant's cellular structure, and in the shortwave infrared, by moisture content. Healthy green vegetation has high reflectance in the near infrared and lower values in the shortwave infrared, especially in the water absorption bands. When vegetation is burned, its reflectance decreases dramatically in the near infrared and increases in the shortwave infrared band. This makes the numerator resultant in equation 1 negative for forest fire scars and positive for vegetated areas.

Figure 5. Spectral behavior of healthy vegetation and burned area.

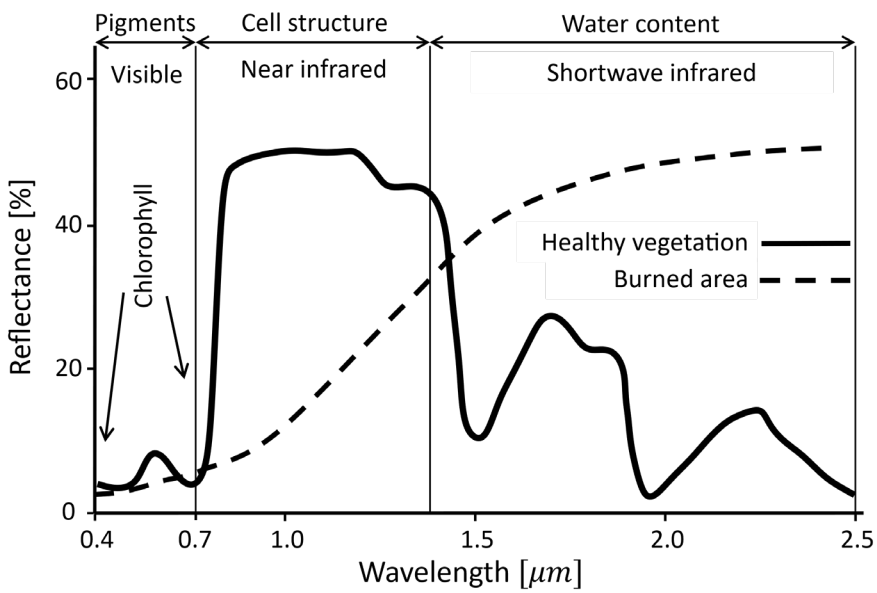

Source: adapted from Alcaras *et al.* (2022).

Various spectral indices can be used to highlight burned areas, particularly the fire index (Barbosa and Fearnside, 2005a, 2005b; Cabral *et al.*, 2018; Fearnside *et al.*, 2009; Fearnside *et al.*, 2007; French *et al.*, 2020; Generous *et al.*, 2007; Hao and Larkin, 2014; Labonne *et al.*, 2007; Roy *et al.*, 2005).

Figure 6 shows the NBR for the study area on July 15, 2023. Calculating this index can be understood as a mathematical operation on geofields, which produces a new numerical geofield with values belonging to the set of real numbers. In this image, pixel values can vary in the range [-1,1]. Thus, pixels with negative values in NBR are strong candidates for forest fire pixels. Pixels with positive values tend to represent healthy vegetation. Note that the minimum value is approximately -0.4, and the maximum value is close to 0.7. The color map used employs dark blue tones for lower values and yellow tones for higher values on the scale. Healthy green vegetation appears in shades of yellow, with higher NBR values, whereas exposed soil pixels appear in medium blue/green hue, and forest fire pixels are represented in dark blue.

In Figure 6, detail (A) highlights a portion of the study area where forest fire scars can be seen, colored dark blue. Comparing detail (A) in Figure 6 with Figure 4, one sees that the burned areas stand out from the surrounding areas in NBR.

In Figure 6, pixels segmented as burned areas are superimposed on the NBR and represented in yellow in detail (B). At present, the accuracy of burned area pixel segmentation is limited to qualitative analysis, performed through visual interpretation.

Figure 6. Burned area index of the study area.

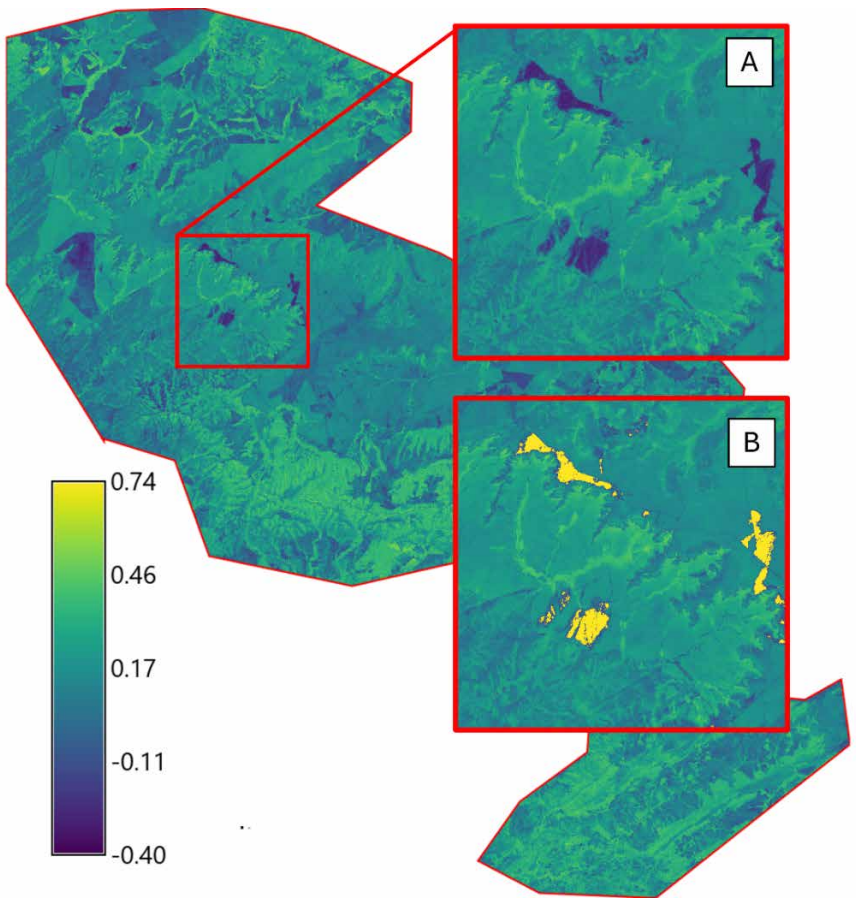

Source: authors (2024).

The burned area for July 15, 2023 was estimated in 707.52 hectares. Using equation 2 and data in Tables 1 to 3, the amount of greenhouse gases released were: CO_2 = 5,249.66 ± 95.01 t; CH_4 = 7.49 ± 1.75 t; and N_2O = 0.68 ± 1.5 t. From September 3, 2023 to August 3, 2024, 70 orbital images were analyzed. The algorithm identified forest fire scars within the PA in June 9, 19 and 29, 2024, July 14, 2024 and August 3, 2024. It shows the evolution of burned areas between May 30, 2024, and June 29, 2024 (Figure 7). The complete image shown was acquired on June 29, 2024. In detail (A), the date prior to the fire is May 30, 2024. An active fire in one of the burning areas can be seen in detail (B), on June 14, 2024. In (C), the maximum expansion of burned areas occurs in the selected areas on June 29, 2024. (D) shows another region on a date prior to the fire, on June 19, 2024. Details (E) and (F) show the scars left by the fire on June 24, 2024 (fire still active) and June 29, 2024.

Table 3 summarizes the results for burned areas and greenhouse gas emissions for the dates of peak scarring. Estimates precision, according to the IPCC methodology, were ± 95.01 for CO_2; ± 1.75 for CH_4; and ± 1.5 for N_2O, in units of tons. Importantly, not all fires occurred simultaneously, which reinforces the need for high temporal resolution for adequate monitoring. Quantification of greenhouse gases can also be achieved using remote sensors (Hasan *et al.*, 2025; Li *et al.*, 2024; Miranda *et al.*, 1994; Moradi and Ghasemifar, 2025; Silva *et al.*, 2018; Zhang *et al.*, 2003).

The system was implemented in a Linux environment using Python language and checks for the presence of burned areas, estimates greenhouse gas emissions, and produces results in the form of maps with pixels belonging to burned areas and tables and graphs with quantities of greenhouse gases emitted. This data, in addition to the calculated spectral indices (such as NBR), is stored in the GIS database and exported to GeoTIFF and CSV formats.

Figure 7. Example of fire evolution in the study area.

Source: authors (2024).

Table 3. Burned areas and their emissions.

Date	Area (ha)	CO_2 (t)	CH_4 (t)	N_2O (t)
June 9, 2024	50.80	376.93	0.54	0.05
June 19, 2024	102.52	760.68	1.08	0.10
June 29, 2024	137.28	1,018.59	1.45	0.13
July 14, 2024	13.68	101.50	0.14	0.01
August 3, 2024	229.37	1,701.88	2.43	0.22

Source: authors (2024).

Conclusions

The fire detection system is operational and performed adequately according to a qualitative analysis of selected images from the study area. Its algorithm identified forest fire scars within the Chapada dos Guimarães PA in June 9, 19 and 29, 2024, July 14, 2024 and August 3, 2024. A total of 533.65 hectares were burned, releasing 3,959.58 tons of CO_2, 5.64 tons of CH_4 and 0.51 tons of N_2O.

NBR spectral index highlights areas where biomass has undergone combustion, enabling the identification of pixels that should be considered as candidates for burned areas. This is because the tests conducted still show false positives in identifying stage results, which occur in areas of well-drained exposed soil. Said identification should be improved by using other spectral indices and/or different methodologies, such as automatic classification and the use of algorithms for detecting changes in time series.

References

ALCARAS, E; COSTANTINO, D.; GUASTAFERRO, F.; PARENTE, C.; PEP, M. Normalized Burn Ratio Plus (NBR+): a new index for Sentinel-2 imagery. **Remote Sensing**, v. 14, n. 7, art. 1727, 2022.

ALVARADO, S. T.; FORNAZARI, T.; COSTOLA, A.; MORELLATO, L. P. C.; SILVA, T. S. Drivers of fire occurrence in a mountainous Brazilian cerrado savanna: tracking long-term fire regimes using remote sensing. **Ecological Indicators**, v. 78, p. 270–281, 2017.

ARGIBAY, D. S.; SPARACINO, J.; ESPINDOLA, G. M. A long-term assessment of fire regimes in a Brazilian ecotone between seasonally dry tropical forests and savannah. **Ecological Indicators**, v. 113, art. 106151, 2020.

ARRUDA, V. L. S.; PIONTEKOWSKI, V. J.; ALENCAR, A.; PEREIRA, R. S.; MATRICARDI, E. A. T. An alternative approach for mapping burn scars using Landsat imagery, Google Earth Engine, and Deep Learning in the Brazilian Savanna. **Remote Sensing Applications Society and Environment**, v. 22, art. 100472, 2021.

ARRUDA, W. DE S.; OLDELAND, J.; FILHO, A. C. P.; CUNHA, N. L.; ISHII, I. H.; DAMASCENO-JUNIOR, G. A. Inundation and fire shape the structure of riparian forests in the Pantanal, Brazil. **PloS one**, v. 11, n. 6, e0156825, 2016.

BARBOSA, R. I.; FEARNSIDE, P. M. Fire frequency and area burned in the Roraima savannas of Brazilian Amazonia. **Forest Ecology and Management**, v. 204, n. 2–3, p. 371–384, 2005a.

BARBOSA, R. I.; FEARNSIDE, P. M. Above-ground biomass and the fate of carbon after burning in the savannas of Roraima, Brazilian Amazonia. **Forest Ecology and Management**, v. 216, n. 1–3, p. 295–316, 2005b.

BASTARRIKA, A.; CHUVIECO, E.; MARTÍN, M. P. Mapping burned areas from Landsat TM/ETM+ data with a two-phase algorithm: balancing omission and commission errors. **Remote Sensing of Environment**, v. 115, n. 4, p. 1003–1012, 2011.

BOSCHETTI, L.; ROY, D. P.; JUSTICE, C. O.; HUMBER, M. L. MODIS–Landsat fusion for large area 30 m burned area mapping. **Remote Sensing of Environment**, v. 161, p. 27–42, 2015.

CABRAL, A. I. R.; SAITO, C.; PEREIRA, H.; LAQUES, A. E. Deforestation pattern dynamics in protected areas of the Brazilian Legal Amazon using remote sensing data. **Applied Geography**, v. 100, p. 101–115, 2018.

CHEN, Y.; MORTON, D. C.; RANDERSON, J. T. Remote sensing for wildfire monitoring: Insights into burned area, emissions, and fire dynamics. **One Earth**, v. 7, n. 6, p. 1022-1028, 2024.

CHUVIECO, E.; MOUILLOT, F.; WERF, G. R.; MIGUEL, J. S.; TANASE, M.; KOUTSIAS, N.; GARCÍA, M.; YEBRA, M.; PADILLA, M.; GITAS, I.; HEIL, A.; HAWBAKER, T. J.; GIGLIO, L. Historical background and current developments for mapping burned area from satellite Earth observation. **Remote Sensing of Environment**, v. 225, p. 45–64, 2019.

DÍAZ-VÁZQUEZ, D.; CASILLAS-GARCÍA, L. F.; GARCIA-GONZALEZ, A.; MONTERO, S. H. G.; RUBUI, J. I. M.; LLAMAS, J. J.; HERNANDEZ, M. S. G. Integrating remote sensing and machine learning for dynamic burn probability mapping in data-limited contexts. **Remote Sensing Applications: Society and Environment**, v. 38, art. 101554, 2025.

FEARNSIDE, P. M.; BARBOSA, R. I.; DE ALENCASTRO GRAÇA, P. M. L. Burning of secondary forest in Amazonia: biomass, burning efficiency and charcoal formation during land preparation for agriculture in Apiaú, Roraima, Brazil. **Forest Ecology and Management**, v. 242, n. 2–3, p. 678–687, 2007.

FEARNSIDE, P. M.; RIGHI, C. A.; GRAÇA, P. M. L. A.; KEIZER, E. W. H.; CERRI, C. C.; NOGUEIRA, E. M.; BARBOSA, R. I. Biomass and greenhouse-gas emissions from land-use change in Brazil's Amazonian "arc of deforestation": The states of Mato Grosso and Rondônia. **Forest Ecology and Management**, v. 258, n. 9, p. 1968–1978, 2009.

FIEDLER, N. C.; MERLO, D. A.; MEDEIROS, M. B. DE. Ocorrência de incêndios florestais no Parque Nacional da Chapada dos Veadeiros, Goiás. **Ciência Florestal**, v. 16, n. 2, p. 153–161, 2006.

FREITAS, W. K.; GOIS, G.; PEREIRA JR., E. R.; JUNIOR, J. F. O.; MAGALHÃES, L. M. S.; BRASIL, F. C.; SOBRAL, B. S. Influence of fire foci on forest cover in the Atlantic Forest in Rio de Janeiro, Brazil. **Ecological Indicators**, v. 115, art. 106340, 2020.

GALANTER, M.; LEVY, H., II; CARMICHAEL, G. R. Impacts of biomass burning on tropospheric CO, NO_2, and O_3. **Journal of Geophysical Research**, v. 105, n. D5, p. 6633–6653, 2000.

GENEROSO, S.; BEY, I.; ATTIÉ, J. K.; BRÉON, F. M. A satellite- and model-based assessment of the 2003 Russian fires: impact on the Arctic region. **Journal of Geophysical Research**, v. 112, n. D15, p. 1-16, 2007.

HAO, W. M.; LARKIN, N. K. Wildland fire emissions, carbon, and climate: wildland fire detection and burned area in the United States. **Forest Ecology and Management**, v. 317, p. 20–25, 2014.

HASAN, H.; ZHANG, P.; CHEN, J.; SHI, G.; ABICHOU, T.; YU, H. Exploring uncertainties in

the integrated mass enhancement method for remote sensing retrievals of methane emissions. **Waste Management**, v. 200, art. 114759, 2025.

HISLOP, S.; HAYWOOD, A.; JONES, S.; SOTO-BERELOV, M.; SKIDMORE, A. K.; NGUYEN, T. H. A satellite data driven approach to monitoring and reporting fire disturbance and recovery across boreal and temperate forests. **International Journal of Applied Earth Observation and Geoinformation**: ITC journal, v. 87, art. 102034, 2020.

ICMBIO. **Plano de manejo do Parque Nacional da Chapada dos Guimarães.** Ministério do Meio Ambiente. [s.l.] Instituto Chico Mendes de Conservação da Biodiversidade, 2009. Disponível em: < https://uc.socioambiental.org/arp/1142 >. Acesso em: 26 jun. 2025.

IPCC. 2019 **Refinement to the 2006 IPCC guidelines for national greenhouse gas inventories.** Suíça: IPCC, 2019. Disponível em: <https://www.ipcc.ch/report/2019-refinement-to-the-2006-ipcc-guidelines-for-national-greenhouse-gas-inventories/>. Acesso em: 26 jun. 2025.

KAUFMAN, Y. J.; SETZER, A.; WARD, D.; TANRE, D.; HOLBEN, B. N.; MENZEL, P.; PEREIRA, M. C.; RASMUSSEN, R. Biomass burning airborne and spaceborne experiment in the Amazonas (BASE-A). **Journal of Geophysical Research**, v. 97, n. D13, p. 14581–14599, 1992.

LABONNE, M.; BRÉON, F.-M.; CHEVALLIER, F. Injection height of biomass burning aerosols as seen from a spaceborne lidar. **Geophysical Research Letters**, v. 34, n. 11, art. L11806, 2007.

LANGMANN, B.; DUNCAN, B.; TEXTOR, C.; TRENTMANN, J.; WERF, G. R. Vegetation fire emissions and their impact on air pollution and climate. **Atmospheric Environment**, v. 43, n. 1, p. 107–116, 2009.

LARIS, P. S. Spatiotemporal problems with detecting and mapping mosaic fire regimes with coarse-resolution satellite data in savanna environments. **Remote Sensing of Environment**, v. 99, n. 4, p. 412–424, 2005.

LI, H.; JIN, X.; ZHAO, R.; HAN, B.; ZHOU, Y.; TITTONELL, P. Assessing uncertainties and discrepancies in agricultural greenhouse gas emissions estimation in China: A comprehensive review. **Environmental Impact Assessment Review**, v. 106, art. 107498, 2024.

MACHADO, R. B.; NETO, M. R.; PEREIRA, P. G.; CALDAS, E. F.; GONÇALVES, D. A.; SANTOS, N.; TABOR, K.; STEININGER, M. Estimativas de perda da área do Cerrado brasileiro. Relatório técnico não publicado. **Conservação Internacional**, Brasília, DF, 2004. Disponível em: < https://jbb.ibict.br/bitstream/1/357/1/2004_%20Conservacao%20Internacional_%20estimativa_desmatamento_cerrado.pdf>. Acesso em: 26 jun. 2025.

MAKINECI, H. B. Investigation of burned areas with multiplatform remote sensing data on the Rhodes 2023 forest fires. **Ain Shams Engineering Journal**, v. 15, n. 10, art. 102949, 2024.

MIRANDA, A. I.; COUTINHO, M.; BORREGO, C. Forest fire emissions in Portugal: a contribution to global warming? **Environmental Pollution**, v. 83, n. 1–2, p. 121–123, 1994.

MOLEMA, T. R.; TESFAMICHAEL, S. G.; FUNDISI, E. Optical and radar remote sensing for burn scar mapping in the grassland biome. **Remote Sensing Applications: Society and Environment**, v. 38, art. 101548, 2025.

MORADI, S.; GHASEMIFAR, E. Analysis of the gas emissions from volcanic activity in the East African Rift System using remote sensing over the past two decades. **Remote Sensing Applications: Society and Environment**, v. 37, art. 101471, 2025.

OLSON, J. R.; BAUM, B. A.; CAHOON, D. R.; CRAWFORD, J. H. Frequency and distribution of forest, savanna, and crop fires over tropical regions during PEM-Tropics A. **Journal of Geophysical Research**, v. 104, n. D5, p. 5865–5876, 1999.

PEREIRA, A. A.; PEREIRA, J. A.; MORELLI, F.; BARROS, D. A.; ACERBI JR, F. W.; SCOLFORO, J. R. S. Validação de focos de calor utilizados no monitoramento orbital de queimadas por meio de imagens TM. **CERNE**, v. 18, n. 2, p. 335–343, 2012.

PLENIOU, M.; KOUTSIAS, N. Sensitivity of spectral reflectance values to different burn and vegetation ratios: a multi-scale approach applied in a fire affected area. **ISPRS Journal of Photogrammetry and Remote Sensing**: official publication of the International Society for Photogrammetry and Remote Sensing (ISPRS), v. 79, p. 199–210, 2013.

ROY, D. P.; GUHA, A.; KUMAR, K. V. An approach of surface coal fire detection from ASTER and Landsat-8 thermal data: Jharia coal field, India. **International Journal of Applied Earth Observation and Geoinformation**: ITC Journal, v. 39, p. 120–127, 2015.

ROY, D. P.; JIN, Y.; LEWIS, P. E.; JUSTICE, C. O. Prototyping a global algorithm for systematic fire-affected area mapping using MODIS time series data. **Remote Sensing of Environment**, v. 97, n. 2, p. 137–162, 2005.

SANO, S. M.; DE ALMEIDA, S. P.; RIBEIRO, J. F. **Cerrado:** ecologia e flora. Parque Estação Biológica - PqEB. Brasília, DF: Embrapa, 2008. 410 p.

SHIMABUKURO, Y. E.; DUTRA, A. C.; ARAI, E.; DUARTE, V.; CASSOL, H. K. G.; PEREIRA, G.; CARDOZO, F. S. Mapping burned areas of Mato Grosso State Brazilian Amazon using multisensor datasets. **Remote Sensing**, v. 12, n. 22, art. 3827, 2020.

SILVA, S. S.; FEARNSIDE, P. M.; GRAÇA, P. M. L. A.; BROWN, I. F.; ALENCAR, A.; MELO, A. W. F. Dynamics of forest fires in the southwestern Amazon. **Forest Ecology and Management**, v. 424, p. 312–322, 2018.

URBANSKI, S. Wildland fire emissions, carbon, and climate: emission factors. **Forest Ecology and Management**, v. 317, p. 51–60, 2014.

VASCONCELOS, S. S.; FEARNSIDE, P. M.; GRAÇA, P. M. L.; NOGUEIRA, E. M.; OLIVEIRA, L. C.; FIGUEIREDO, E. O. Forest fires in southwestern Brazilian Amazonia: estimates of area and potential carbon emissions. **Forest Ecology and Management**, v. 291, p. 199–208, 2013.

WOOSTER, M. J.; ROBERTS, G.; PERRY, G. L.; KAUFMAN, Y. J. Retrieval of biomass combustion rates and totals from fire radiative power observations: FRP derivation and calibration relationships between biomass consumption and fire radiative energy release. **Journal of Geophysical Research**, v. 110, n. D24, p. 1-24, 2005.

ZHANG, Y.-H.; WOOSTER, M. J.; TUTUBALINA, O.; PERRY, G. L. Monthly burned area and forest fire carbon emission estimates for the Russian Federation from SPOT VGT. **Remote Sensing of Environment**, v. 87, n. 1, p. 1–15, 2003.